Human Molecular Genetics, 2023, Vol. 32, 24, 3374–3389
https://doi.org/10.1093/hmg/ddad164
Advance access publication date 26 September 2023
Original Article

Identification of a muscle-specific isoform of VMA21 as a potent actor in X-linked myopathy with excessive autophagy pathogenesis

Ilaria Cocchiararo[1], Olivia Cattaneo[1], Jayasimman Rajendran[1], Florent Chabry[1], Mélanie Cornut[1], Hadrien Soldati[1], Anne Bigot[2], Kamel Mamchaoui[2], Sara Gibertini[3], Axelle Bouche[1,4], Daniel J. Ham[5], Thomas Laumonier[1,4], Alexandre Prola[1], Perrine Castets[1,*]

[1]Department of Cell Physiology and Metabolism, Faculty of Medicine, University of Geneva, 1 rue Michel Servet, CH-1211 Geneva, Switzerland
[2]Centre de Recherche en Myologie, Inserm, Institut de Myologie, Sorbonne Université, 47 Bd de l'Hôpital, 75013 Paris, France
[3]Neuromuscular Diseases and Neuroimmunology Unit, Muscle Cell Biology Lab, Fondazione IRCCS Istituto Neurologico "C. Besta", Via Amadeo 42, 20133 Milano, Italy
[4]Department of Orthopaedic Surgery, Geneva University Hospitals and Faculty of Medicine, University Medical Center, 1 rue Michel Servet, 1211, Geneva, Switzerland
[5]Biozentrum, University of Basel, Spitalstrasse 41, 4056 Basel, Switzerland

*Corresponding author. Department PHYM, Centre Médical Universitaire de Genève, 1 rue Michel Servet, CH-1211 Genève, Suisse. E-mail: perrine.castets@unige.ch

Abstract

Defective lysosomal acidification is responsible for a large range of multi-systemic disorders associated with impaired autophagy. Diseases caused by mutations in the *VMA21* gene stand as exceptions, specifically affecting skeletal muscle (X-linked Myopathy with Excessive Autophagy, XMEA) or liver (Congenital Disorder of Glycosylation). VMA21 chaperones vacuolar (v-) ATPase assembly, which is ubiquitously required for proper lysosomal acidification. The reason VMA21 deficiencies affect specific, but divergent tissues remains unknown. Here, we show that *VMA21* encodes a yet-unreported long protein isoform, in addition to the previously described short isoform, which we name VMA21-120 and VMA21-101, respectively. In contrast to the ubiquitous pattern of VMA21-101, VMA21-120 was predominantly expressed in skeletal muscle, and rapidly up-regulated upon differentiation of mouse and human muscle precursors. Accordingly, VMA21-120 accumulated during development, regeneration and denervation of mouse skeletal muscle. In contrast, neither induction nor blockade of autophagy, *in vitro* and *in vivo*, strongly affected VMA21 isoform expression. Interestingly, VMA21-101 and VMA21-120 both localized to the sarcoplasmic reticulum of muscle cells, and interacted with the v-ATPase. While VMA21 deficiency impairs autophagy, VMA21-101 or VMA21-120 overexpression had limited impact on autophagic flux in muscle cells. Importantly, XMEA-associated mutations lead to both VMA21-101 deficiency and loss of VMA21-120 expression. These results provide important insights into the clinical diversity of *VMA21*-related diseases and uncover a muscle-specific VMA21 isoform that potently contributes to XMEA pathogenesis.

Keywords: XMEA; autophagy; myogenesis; VMA21; v-ATPase

Introduction

Macroautophagy (thereafter referred to as autophagy) ensures the degradation and turnover of organelles and proteins in cells [1] and has become a key targetable process in several pathological conditions. In skeletal muscle, autophagy must be tightly controlled to maintain homeostasis. Indeed, excessive autophagic flux causes muscle degeneration and atrophy [2, 3]. On the other hand, impaired flux promotes the accumulation of damaged organelles and autophagic vacuoles, thereby contributing to muscle wasting and weakness [3, 4]. Despite detailed molecular characterization of the autophagic machinery and its associated regulatory pathways, our capacity to normalize autophagic flux in muscle diseases remains limited.

Autophagic Vacuolar Myopathies (AVMs) are rare neuromuscular disorders associated with impaired autophagic degradation, including Danon and Pompe diseases, which are caused by mutations in the lysosomal genes, *LAMP2* and *GAA*, respectively [5]. In 2013, mutations in the *VMA21* gene were shown to cause X-linked Myopathy with Excessive Autophagy (XMEA; OMIM #310440), another rare AVM [6]. XMEA patients show early- to late- disease onset with muscle-specific dysfunction marked by atrophy and weakness [7]. Results in yeast indicate VMA21 (i.e. Vma21p) plays an important role in chaperoning vacuolar (v-) ATPase assembly. v-ATPase is a proton pump formed by a membranous V0 domain, containing $ac_8c'c''$def (yeast) or ac_xc''de (mammals) sub-units, and a cytosolic enzymatic V1 domain, containing $A_3B_3CDE_3FG_3H$ sub-units [6, 8–10]. Genetic deficiencies in v-ATPase sub-units or accessory proteins are responsible for a large group of disorders related to defective lysosomal acidification [11]. Depending on the expression pattern

Received: June 8, 2023. **Revised:** August 23, 2023. **Accepted:** September 21, 2023

of the mutated gene, these multi-systemic diseases can involve neurological, liver, bone, skin, kidney, immune and/or metabolic dysfunctions. In contrast, disease symptoms in XMEA are restricted to skeletal muscle tissue, with only rare observations of liver dysfunction or sub-clinical heart involvement [12–15]. This is surprising given the ubiquitous expression of VMA21 and its role in assembling the V0 domain within the endoplasmic reticulum (ER) before V0/V1 complex formation. Intriguingly, in 2020, congenital liver disease related to defective glycosylation (CDG) were also shown to result from mutations in *VMA21*, despite no reported sign of myopathy [16]. How *VMA21* mutations selectively impair skeletal muscle in XMEA, while affecting the liver in CDG, remains a mystery. More recently, follicular lymphoma has also been associated with mutations in *VMA21* [17], further expanding the clinical spectrum of *VMA21*-related diseases.

In this study, we characterize *in silico*-predicted VMA21 isoforms, unveiling the expression of two main isoforms in mouse and human, with one of them predominantly expressed in skeletal muscle. While each isoform displayed distinct expression patterns during myogenesis, their sub-cellular distribution was similar, showing an enrichment within the sarcoplasmic reticulum (SR) of muscle fibers. Importantly, both isoforms are lost in skeletal muscle cells from XMEA patients, indicating that the newly identified muscle-specific isoform of VMA21 likely contributes to disease pathophysiology.

Results

Alternative transcription start sites lead to different VMA21 isoforms

Genome and protein browsers predicted two VMA21 isoforms in humans, hereafter referred to as VMA21-101 (Uniprot: Q3ZAQ7, NCBI: NP_001017980.1, Ensembl: ENST00000330374.7) and VMA21-156 (NP_001350739.1, ENST00000370361.5), based on the number of amino acids in the protein sequence. Four isoforms were predicted in mice, referred to as VMA21-101 (Q78T54, NP_001074825.1, ENSMUST00000114576.9), VMA21-120 (F2Z446, NP_001277710.1, ENSMUST00000114577.8), VMA21-134 (F2Z447, NP_001277709.1, ENSMUST00000114575.4), and VMA21-161 (a putative isoform only present on NCBI: XP_006528324.1). Previous reports focus on the *VMA21-101* transcript, which is composed of 3 exons (Fig. 1A). The other transcripts arise from alternative transcription start sites (TSS), located upstream or downstream of the *VMA21-101* TSS (Fig. 1A). Therefore, the transcripts share exons 2 and 3, but have a unique exon 1 sequence (Fig. 1A). In humans, *VMA21-156* encompasses a putative *VMA21-120* transcript, with an ATG codon within *VMA21-156* exon 1 equivalent to the one present in mice (Fig. 1A). As they share the same sequences, including 5′UTR/exon1 regions, *VMA21-120* and *-156* transcripts cannot be selectively amplified. A PCR on cDNA from muscle cells confirmed the transcriptional expression of *VMA21-101* and *-120/156* in humans, and of *Vma21-101*, *-120*, and *-134* in mice (Fig. 1B and C). In mice, *Vma21-134* was undetectable when using PCR targeting both *Vma21-101* and *-134*, and the band obtained with primers targeting only *Vma21-134* remained barely detectable even with a high number of PCR cycles (Fig. 1B and C). Similarly, the putative *Vma21-161* transcript, encompassing *Vma21-120* (Fig. 1A), was undetectable in mouse cells by PCR with primers targeting the predicted 5′UTR region.

VMA21 protein isoforms differ in their N-terminal regions (Fig. 1D). VMA21-101 is highly conserved throughout evolution (Fig. 1D). On the other hand, sequence similarities within the N-terminal regions are found in mammals for VMA21-120 and in primates only for VMA21-156 (Fig. 1D). There was no sequence homology found within the N-terminal region of VMA21-134 in any other species than mouse. To assess the electrophoretic properties of each VMA21 isoform, we overexpressed mouse VMA21-101, -120, -134 and human VMA21-156 isoforms in C2C12 cells. Commercial antibodies designed against N- (specific; Ab101 and Ab120) and C- (common; Pan) terminal regions recognized the corresponding protein isoform or all isoforms, respectively (Fig. 1E). VMA21-101, -120, -134 and VMA21-156 migrated at their expected sizes (11.5, 13.5, 15 and 18 kDa, respectively; Fig. 1E). The 10 kDa protein detected when overexpressing VMA21-134 likely arose from proteolytic cleavage of VMA21-134 (Fig. 1E). Specificity of the antibodies was further confirmed by immunostaining of VMA21-overexpressing cells (Supplementary Material, Fig. S1). Together, these results indicate that expression of the *VMA21* gene gives rise to at least two different transcripts, *VMA21-101* and *VMA21-120/156*, in human and rodent cells.

VMA21 isoforms are differentially expressed in skeletal muscle and non-muscle tissues

To determine the expression pattern of each VMA21 isoform, we first performed a PCR targeting full-length *Vma21* transcripts (mPCR1a/1b/2; Fig. 1B) in liver, brain, kidney, lung, skeletal muscles (i.e. *tibialis anterior* (TA), *gastrocnemius* (GA), *soleus*, diaphragm) and heart from 3-month-old mice (Fig. 2A). While *Vma21-101* expression was clearly detected in all tissues, the PCR product for *Vma21-134* was detected in brain, kidney, lung and diaphragm (using more PCR cycles) but was barely detectable in all other tissues. Similarly, *Vma21-120* expression was observed in all skeletal muscles, but was undetectable in all non-skeletal muscle tissues (Fig. 2A). By quantitative PCR, total *Vma21* mRNA levels (Pan; Fig. 2B) were higher in muscles than non-muscle tissues (Fig. 2C). When normalized to total *Vma21* expression, *Vma21-101* expression was highest in non-muscle tissues (Fig. 2D), while *Vma21-120* expression was predominantly detected in TA, GA, *soleus* and diaphragm, with intermediate expression in the heart (Fig. 2E). Brain tended to express *Vma21-134* at higher levels than other tissues, although this isoform was overall more difficult to amplify by qPCR (Fig. 2F). In support of these observations, RNAseq data available on the *WashU Epigenome Browser* [18, 19] confirmed that *Vma21-120* is expressed predominantly, if not exclusively, in skeletal muscle, while *Vma21-101* is detected in all tissues (Supplementary Material, Fig. S2A). There was no read corresponding to *Vma21-134* exon 1 in any tissue examined, confirming that this isoform is not (or barely) expressed in mice (Supplementary Material, Fig. S2A).

Using antibodies against VMA21-101 or VMA21-120, we confirmed ubiquitous tissue expression of VMA21-101 in mice, with the highest levels detected in liver, brain and lung (Fig. 2G and H), and higher levels in diaphragm and heart, as compared to other muscles (Fig. 2I). Consistent with mRNA levels, VMA21-120 was detected only in muscles, with high and low levels observed in skeletal muscles and heart, respectively (Fig. 2G, J and K). VMA21-120 levels were lower in *soleus* and diaphragm, compared to TA muscle. Of note, smaller bands detected for VMA21-101 and VMA21-120 in *soleus* and/or heart may correspond to cleaved forms of the proteins (Fig. 2G). To confirm this expression pattern, we conducted immunoprecipitation of VMA21-120 with Ab120 from mouse tissues. In these conditions, VMA21-120 was detected in muscles, with higher levels in TA muscle and very low levels in heart (Supplementary Material, Fig. S2B). In striking contrast, only traces of VMA21-120 were detectable in lung, brain and liver,

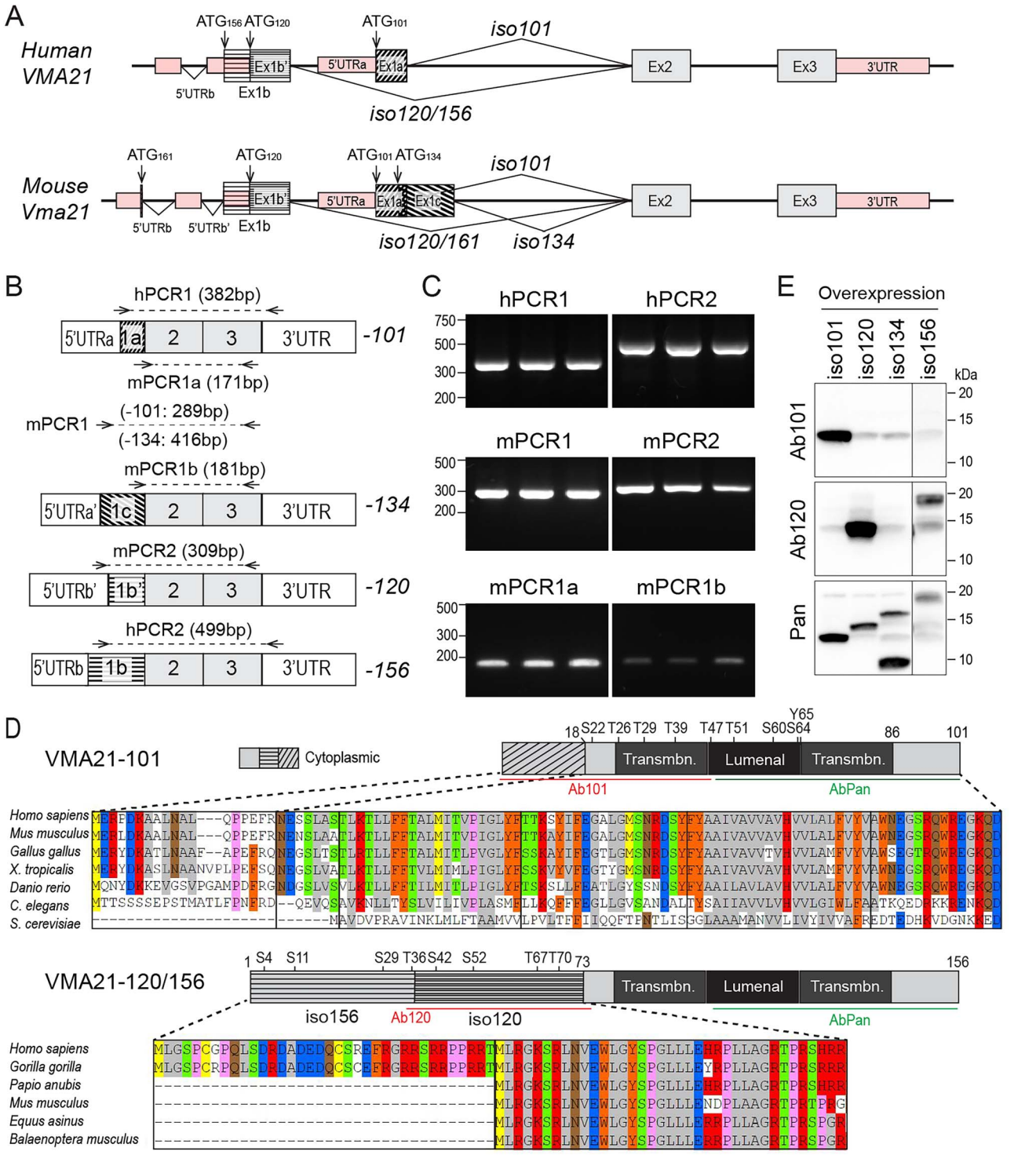

Figure 1. Characterization of human and mouse VMA21 isoforms. (A and B) Organization of *VMA21/Vma21* genes (A) and mRNA (B) in human (h) and mouse (m). Exons, introns and untranslated (UTR) sequences are represented by stripped or gray boxes, black lines and red boxes, respectively. Alternative ATG codons are indicated with arrows. Primers used for PCR are shown on top of mRNA with the size of the amplicons (B). (C) Expression of *VMA21-101/-156* (hPCR1/2) and *Vma21-101/120/134* (mPCR1/1a/1b/2) is detected in primary human (h) and mouse (m) myoblasts by PCR. n = 3 independent samples. (D) Predicted protein domains of VMA21-101 and -120/156. Sequence similarity is found for VMA21-101 from human to *Caenorhabditis elegans*. The N-terminal region of VMA21-101 does not share sequence similarity with Vma21p of *Saccharomyces cerevisiae*. Sequence similarities with the N-terminal regions of VMA21-120 and of VMA21-156 are found in mammals and only in primates, respectively. Amino acid numbers and putative phosphorylation sites are indicated above the domains. Amino acids are colored depending on their physicochemical properties (aliphatic (A, I, L, V); aromatic (F, W, Y); with sulfur (M); hydroxyl (S, T); positively charged (H, K, R); negatively charged (D, E); acidic uncharged (N, Q); heterocyclic (P)). Regions recognized by antibodies Ab101, Ab120 and pan are shown below the protein domains. *Transmbn*: *Transmembrane*. (E) Western blot analysis of VMA21 isoforms in C2C12 cells overexpressing mouse VMA21-101, -120, -134 and human VMA21-156. Antibodies are directed against VMA21-101 (Ab101), VMA21-120/156 (Ab120) or all VMA21 isoforms (pan). VMA21-156 was not run on the same gel.

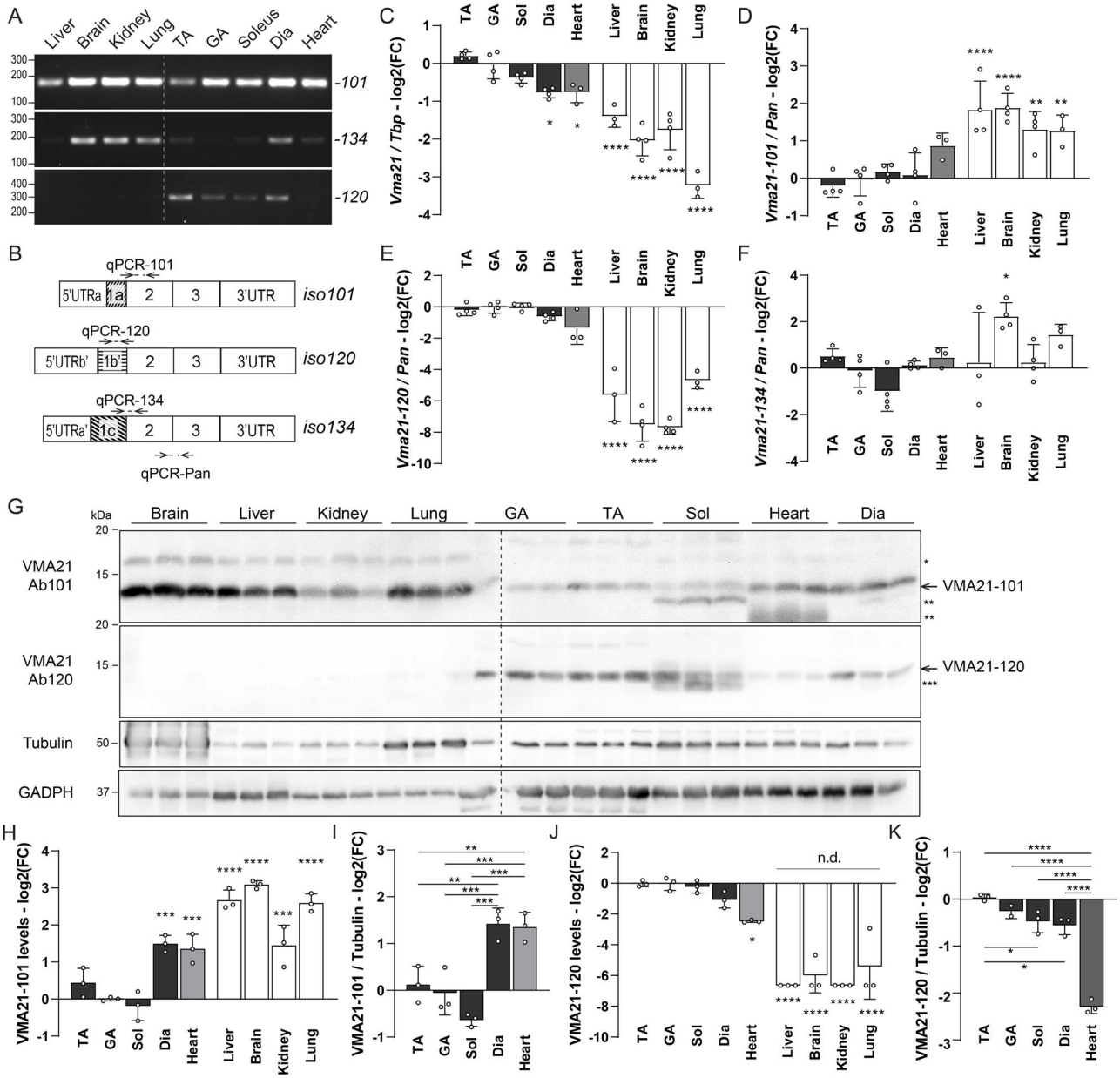

Figure 2. Skeletal muscles express a long isoform of VMA21. (A) End-point PCR shows expression of *Vma21* isoforms in tissues isolated from 3-month-old mice. Representative of at least 3 independent experiments. (B) Primers designed for specific amplification of *Vma21* isoforms by qPCR. (C–F) Levels of total *Vma21* mRNA (C) and of *Vma21-101* (D), *Vma21-120* (E), *Vma21-134* (F) transcripts in muscle and non-muscle tissues from 3-month-old mice. Levels are relative to *Tbp* mRNA (C) or to total *Vma21* mRNA (D–F), and normalized to GA muscle. (G–K) Western blot analysis of VMA21 isoforms in non-muscle and muscle tissues from 3-month-old mice. The band above 15 kDa detected with Ab101 (one asterisk) is unlikely to be VMA21-134, based on the specific pattern obtained with overexpressing cells. Bands detected below VMA21-101 and VMA21-120, with Ab101 (2 asterisks) and Ab120 (3 asterisks) may correspond to cleaved forms of the proteins. Absolute quantification of VMA21-101 and -120 is given in H and J, respectively. For muscles, levels of VMA21-101 and -120 normalized to tubulin and to GA levels are given in I and K, respectively. *n.d.: not detected; TA: tibialis anterior; GA: gastrocnemius, Sol: soleus, Dia: diaphragm.* All values are mean ± SD; n = 4 (C–F; except for heart, liver and lung: n = 3); 3 (G-K); *p < 0.05, **p < 0.01, ***p < 0.001, ****p < 0.0001, one-way ANOVA with Dunnett's post-hoc analysis as compared to GA muscle (C–F, H, J) and one-way ANOVA with Tukey's post-hoc analysis (I, K).

but not in kidney (Supplementary Material, Fig. S2B). Together, these results reveal tissue-specific VMA21 isoform expression patterns, with VMA21-120 predominantly expressed in skeletal muscle.

Differentiating muscle cells strongly up-regulate VMA21-120

To further characterize the VMA21 isoform expression patterns in skeletal muscle, we assessed their transcript and protein levels during myogenesis. Total *Vma21* mRNA levels strongly increased upon differentiation of C2C12 cells (Fig. 3A). This coincided with a striking up-regulation of *Vma21-120* (Fig. 3B), while *Vma21-101* levels remained largely unchanged (Fig. 3C). Changes in *Vma21-120* expression correlated with up-regulation of *Myog*, which encodes the myogenic differentiation marker Myogenin (Fig. 3D). The increase in total *Vma21* and *Vma21-120* levels was observed alongside *Myog* expression within 24 h of switching myoblasts to differentiation medium (i.e. prior to myotube formation; Supplementary Material, Fig. S3A). At the protein level, VMA21-120 was undetectable in C2C12 myoblasts, but

accumulated strongly at differentiation day 2 and 4, while VMA21-101 remained unchanged upon differentiation (Fig. 3E).

To confirm these results, we examined VMA21 expression in primary mouse muscle cells. VMA21-101 and VMA21-120 were both detected at low levels in primary myoblasts in growth condition (Fig. 3F). Importantly, and in line with observations in C2C12 cells, differentiation also strongly increased VMA21-120 levels (Fig. 3F). The expression pattern of VMA21-120 followed the expression kinetics of Myogenin in C2C12 and primary muscle cells (Fig. 3E and F). These results confirmed the up-regulation of VMA21-120 upon muscle precursor commitment and differentiation. Consistent with Western blot results, we observed that few primary muscle cells, under growth conditions, stained positive for VMA21-120, while all of them were positive for VMA21-101 staining (Fig. 3G). To determine whether this small population of VMA21-120-positive cells corresponds to committed muscle cells, we co-stained primary myoblasts for the muscle differentiation markers myosin and SERCA1. Indeed, most VMA21-120-positive cells co-stained for myosin or SERCA1, indicating that these myoblasts spontaneously commit to differentiation despite growth medium conditions (Fig. 3H). This was consistent with the detection of low Myogenin levels in primary myoblasts under growth conditions (Fig. 3F). Therefore, VMA21-120 may be an early marker of myogenic differentiation. To confirm this result, we compared VMA21-120 immunostaining on C2C12 cells seeded at low confluency and kept in growth conditions, or seeded at low and high confluences before switching to differentiation medium. Low confluency allows differentiation but prevents muscle cell fusion when switched to low serum conditions [20]. Under growth conditions (i.e. proliferating cells), C2C12 myoblasts were negative for VMA21-120. In contrast, after 3 days in differentiation media, a large proportion of C2C12 cells seeded at low confluency (i.e. mononucleated cells) co-stained for VMA21-120 and myosin (Fig. 3I). Similarly, highly confluent cells formed myotubes (i.e. fused cells) in differentiation media and also stained positive for VMA21-120 (Fig. 3I). Therefore, VMA21-120 expression is rapidly induced during muscle precursor differentiation, irrespective of fusion. These results are supported by publicly available RNAseq data [18, 19] (Supplementary Material, Fig. S3B) and by the identification of several E-box consensus sites in the 5′UTR region of *Vma21-120* (Supplementary Material, Fig. S3C). Published ChIPseq data [18, 19] also confirmed MyoD1 and Myogenin binding within corresponding regions in committed muscle cells (i.e. myocyte; Supplementary Material, Fig. S3C). Overall, these data show that VMA21-120 is predominantly expressed in differentiating muscle precursors and in skeletal muscle.

VMA21 isoform expression varies during muscle development and regeneration

As the VMA21-120 isoform was strongly expressed upon muscle cell differentiation *in vitro*, we assessed its expression pattern during development and regeneration of mouse skeletal muscle. VMA21-101 and VMA21-120 levels decreased from embryonic stage E16.5 to 3 months of age in mouse TA muscle (Fig. 4A) and diaphragm (Supplementary Material, Fig. S4A), before stabilizing out to 22–24 months of age. Inversely, levels of both isoforms were strongly increased following $BaCl_2$-induced muscle injury (Fig. 4B). VMA21-101 levels peaked 3 days after injury (Fig. 4B) when immune cells and undifferentiated muscle cells accumulate (Supplementary Material, Fig. S4B). On the other hand, VMA21-120 expression was elevated 7 days after injury (Fig. 4B), concomitant with nascent muscle fiber formation (Supplementary Material, Fig. S4B). Immunostaining of injured muscle showed a strong signal for both VMA21-101 and -120 in mononucleated cells, 3 days after injury (Supplementary Material, Fig. S4C). Strong VMA21-101 staining was detected in CD11b-positive immune cells, including macrophages (Supplementary Material, Fig. S4D), while weaker staining was also observed in Desmin-positive mononucleated cells (i.e. muscle precursors; Fig. 4C). In contrast, VMA21-120 staining was observed 3 days after injury specifically in Desmin-positive muscle cells and regenerating fibers (Fig. 4C and Supplementary Material, Fig. S4C), but not in immune cells (Supplementary Material, Fig. S4D). VMA21-120-positive cells were negative for the myogenic marker Pax7, expressed in proliferating and self-renewing muscle cells at this stage (Supplementary Material, Fig. S4E). In contrast, most VMA21-120-positive cells were also stained positive for Myogenin, corresponding to differentiating muscle cells (Supplementary Material, Fig. S4E). Seven days after injury, VMA21-120 accumulated in perinuclear regions of newly formed muscle fibers (Supplementary Material, Fig. S4C). These results confirm that the VMA21-120 isoform is predominantly expressed upon commitment, differentiation and maturation of muscle cells during development and regeneration of skeletal muscle.

As denervation induces the re-expression of myogenic markers, such as Myogenin [21, 22], we lastly assessed the expression pattern of VMA21 isoforms in muscle after sciatic nerve cut. The expression of VMA21-101 was unchanged upon nerve injury (Fig. 4D and Supplementary Material, Fig. S4F) and was detected in muscle fibers and interstitial cells, within both innervated and denervated muscles (Fig. 4E). On the other hand, denervation strongly increased transcript and protein levels of VMA21-120 (Fig. 4D and Supplementary Material, Fig. S4F). In both innervated and denervated muscles, VMA21-120 staining was observed within perinuclear regions of muscle fibers, but not in interstitial cells (Fig. 4E). VMA21-120 up-regulation is consistent with the re-induction of embryonic programs in denervated adult muscle fibers (Supplementary Material, Fig. S4F) [23] and the presence of E-boxes in the 5′UTR region of *Vma21-120*. Together, these results indicate that the myogenic program coincides with a specific up-regulation of the VMA21-120 isoform, while the ubiquitously expressed VMA21-101 remains largely stable.

Autophagy modulation has minor effects on VMA21 expression

Previous reports suggest that autophagic flux increases during muscle cell differentiation [24, 25]. Therefore, we assessed whether the observed VMA21 isoform expression patterns during myogenesis are related to changes in autophagy. To this end, we treated C2C12 myoblasts and myotubes with chloroquine, a widely used autophagic degradation inhibitor. Protein levels of the autophagic marker LC3II were higher in myotubes than myoblasts, especially with chloroquine treatment, confirming higher autophagic flux in differentiated muscle cells (Supplementary Material, Fig. S5A and B). Moreover, the expression of some (*Map1lc3b* and *Ctsl*, encoding LC3B and Cathepsin L, respectively; Supplementary Material, Fig. S5C and D), but not all (e.g. *Gabarapl1*; Supplementary Material, Fig. S5E) autophagy genes increased upon muscle cell differentiation, as observed for *Vma21-120*. The expression of some v-ATPase sub-units was also up-regulated in myotubes, as compared to myoblasts (Supplementary Material, Fig. S5F and G).

To test the effect of manipulating autophagic flux on VMA21 expression, we treated C2C12 cells with insulin or AZD8055, to activate and inhibit mTORC1, respectively, and thereby block and increase autophagy induction. Treatments were combined

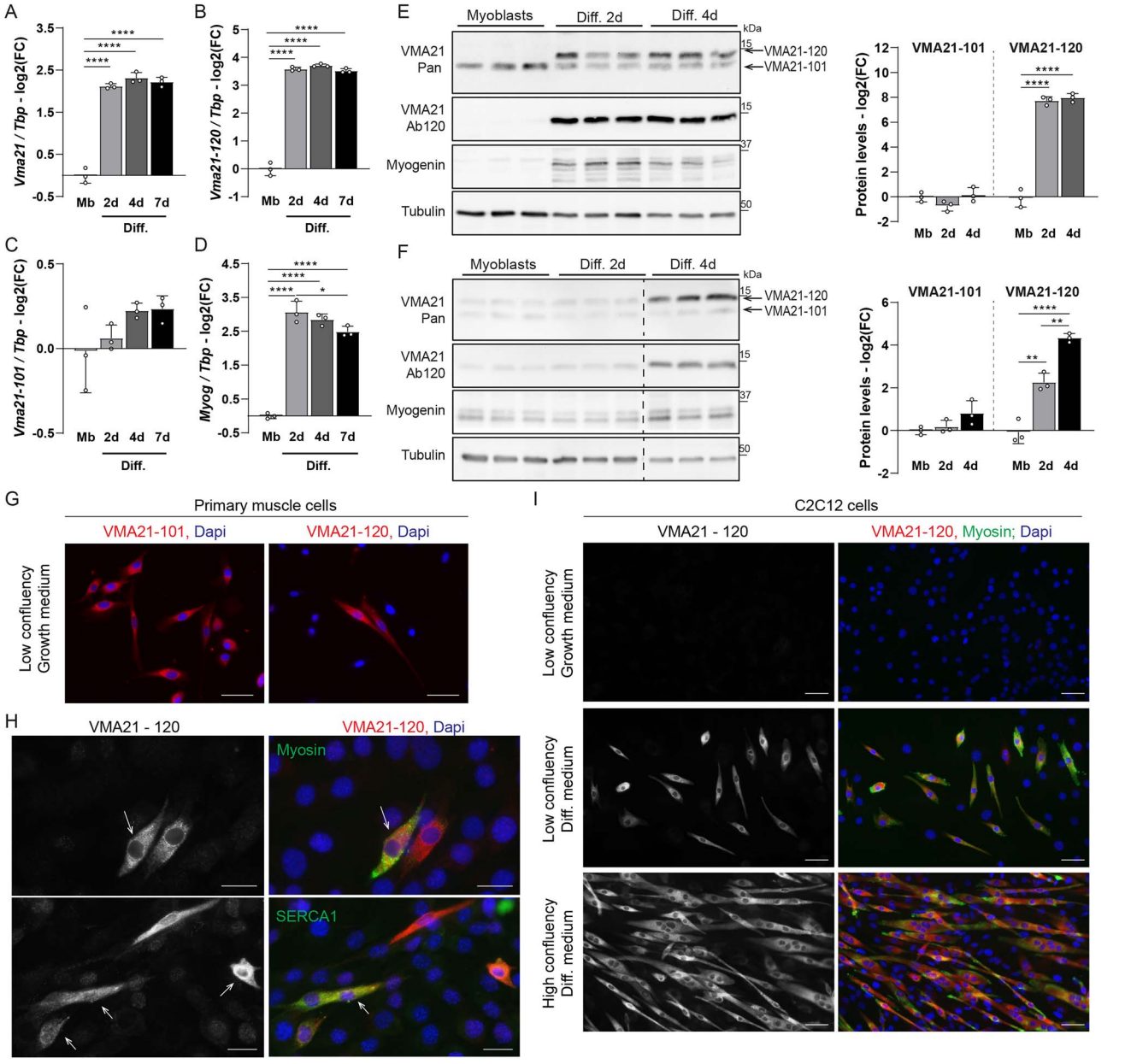

Figure 3. VMA21 isoforms display distinct expression patterns upon muscle cell differentiation. (A–D) mRNA levels of *Vma21* (pan—A), *Vma21-120* (B), *Vma21-101* (C) and *Myog* (D) in C2C12 myoblasts (Mb) and myotubes after 2, 4 and 7 days (d) of differentiation (Diff). Levels are relative to *Tbp* mRNA and to myoblasts. (E, F) Western blot analysis of VMA21 isoforms and Myogenin in C2C12 (E) and primary (F) myoblasts and myotubes after 2 and 4 days (d) of differentiation (Diff). Levels of VMA21-101 and -120 levels are normalized to tubulin and to myoblasts. (G and H) Immunostaining shows expression of VMA21-101 in all primary myoblasts, while VMA21-120 is detected only in some of them in growth conditions (G). Some VMA21-120-positive muscle cells are also positive for myosin and/or SERCA1 (H—Arrows). Scale bar, 50 (G) and 25 (H) μm. (I) Immunostaining shows accumulation of VMA21-120 in C2C12 cells seeded at low (unfused) and high (fused) confluency after 3 days in differentiation medium. Myoblasts in growth medium are negative for VMA21-120. Scale bar, 50 μm. All values are mean ± SD; n = 3; *p < 0.05, **p < 0.01, ****p < 0.0001, one-way ANOVA with Tukey's post-hoc analysis.

with chloroquine to prevent autophagic degradation. VMA21-101 expression was unaffected by insulin, AZD8055 or chloroquine in C2C12 myoblasts (Supplementary Material, Fig. S5H and I). Similarly, mTORC1-mediated autophagy inhibition (insulin) or induction (AZD8055) did not affect VMA21 isoform expression in myotubes (Fig. 5A and B). However, inhibition of autophagic degradation with chloroquine increased VMA21-101 levels and decreased VMA21-120 levels (Fig. 5A and B).

As starvation is a prominent physiological inducer of autophagic flux [2, 3], we next analyzed VMA21 expression in skeletal muscle of mice starved for 24 h or 40 h. Autophagic degradation was blocked with colchicine, as previously shown [3]. While starvation strongly induced autophagic genes, such as *Gabarapl1* (Supplementary Material, Fig. S5J), *Vma21-101* expression was relatively unchanged and *Vma21-120* levels were lower in muscle after 24 h or 40 h of starvation (Fig. 5C). Despite starvation triggering a shift from LC3I to LC3II, confirming increased autophagy (Fig. 5D and Supplementary Material, Fig. S5K), protein levels of VMA21-101/-120 were unchanged by 40 h of starvation and/or colchicine treatment, compared to basal conditions (Fig. 5D and E). Together, these results clearly demonstrate that autophagic activity has limited effects on VMA21-101/-120 expression, unless

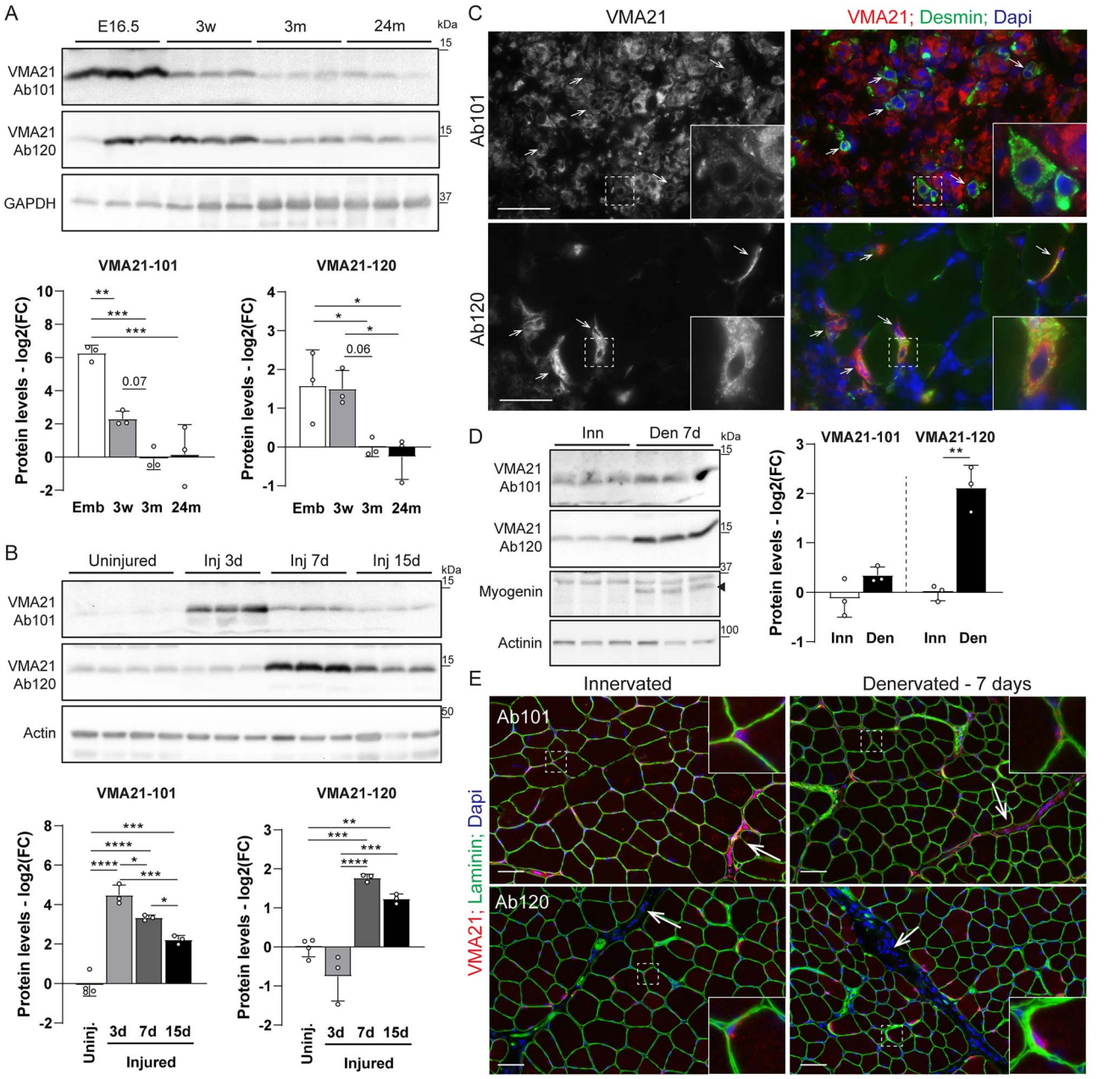

Figure 4. VMA21 isoforms are dynamically expressed during muscle development and regeneration. (A) Western blot analysis of VMA21 isoforms in hindlimb from E16.5 mouse embryos and in TA muscle from 3-week-, 3-month-, and 24-month-old mice. Protein levels are normalized to GAPDH, and relative to 3-month-old mice. *Emb: E16.5; w: week, m: months*. (B) Western blot analysis of VMA21 isoforms in uninjured (Uninj) and injured (Inj) TA muscles, 3, 7 and 15 days after $BaCl_2$-induced injury. Protein levels are normalized to actin, and relative to uninjured muscle. *d: days*. (C) Immunostaining of 3-day-injured muscle sections with Ab101 and Ab120 reveals accumulation of VMA21-101 and -120 in Desmin-positive muscle cells. Arrows indicate muscle cells co-stained for VMA21 and Desmin. Scale bar, 50 μm. (D) Western blot analysis of VMA21 isoforms and Myogenin in innervated (Inn) and denervated (Den) TA muscles, 7 days after sciatic nerve injury. Protein levels are normalized to Actinin, and relative to innervated muscle. *d: days*. (E) Immunostaining with Ab101 and Ab120 shows accumulation of VMA21-101 and -120 in the perinuclear regions of muscle fibers in innervated and denervated muscles. Arrows point to interstitial cells. Scale bar, 50 μm. All values are mean ± SD; n = 3 except for uninjured muscle (n = 4, B); *p < 0.05, **p < 0.01, ***p < 0.001, ****p < 0.0001, one-way ANOVA with Tukey's post-hoc analysis (A and B) or Student's t-test (D).

lysosomal function is directly targeted with drugs, such as chloroquine.

VMA21-120 resides within the ER/SR and interacts with the V0c sub-unit of the v-ATPase

VMA21 was previously shown to reside within the ER, COPII vesicles and the ER-Golgi intermediate compartment (ERGIC) in C2C12 myoblasts [6]. To gain further insight into the respective roles of the VMA21-101 and VMA21-120 isoforms, we analyzed their sub-cellular localization in muscle cells. In myoblasts and myotubes, VMA21-101 staining partially overlapped with staining for the ER marker KDEL (Fig. 6A) and the COPII marker Sec31 (Supplementary Material, Fig. S6A and B). In contrast, VMA21-101 staining did not co-localize with markers for Golgi, COPI, lysosomes or mitochondria (Supplementary Material, Fig. S6A and B). In myotubes, VMA21-120 showed clear perinuclear accumulation, with a sub-cellular distribution comparable to KDEL (Fig. 6A) and Sec31 (Supplementary Material, Fig. S6C).

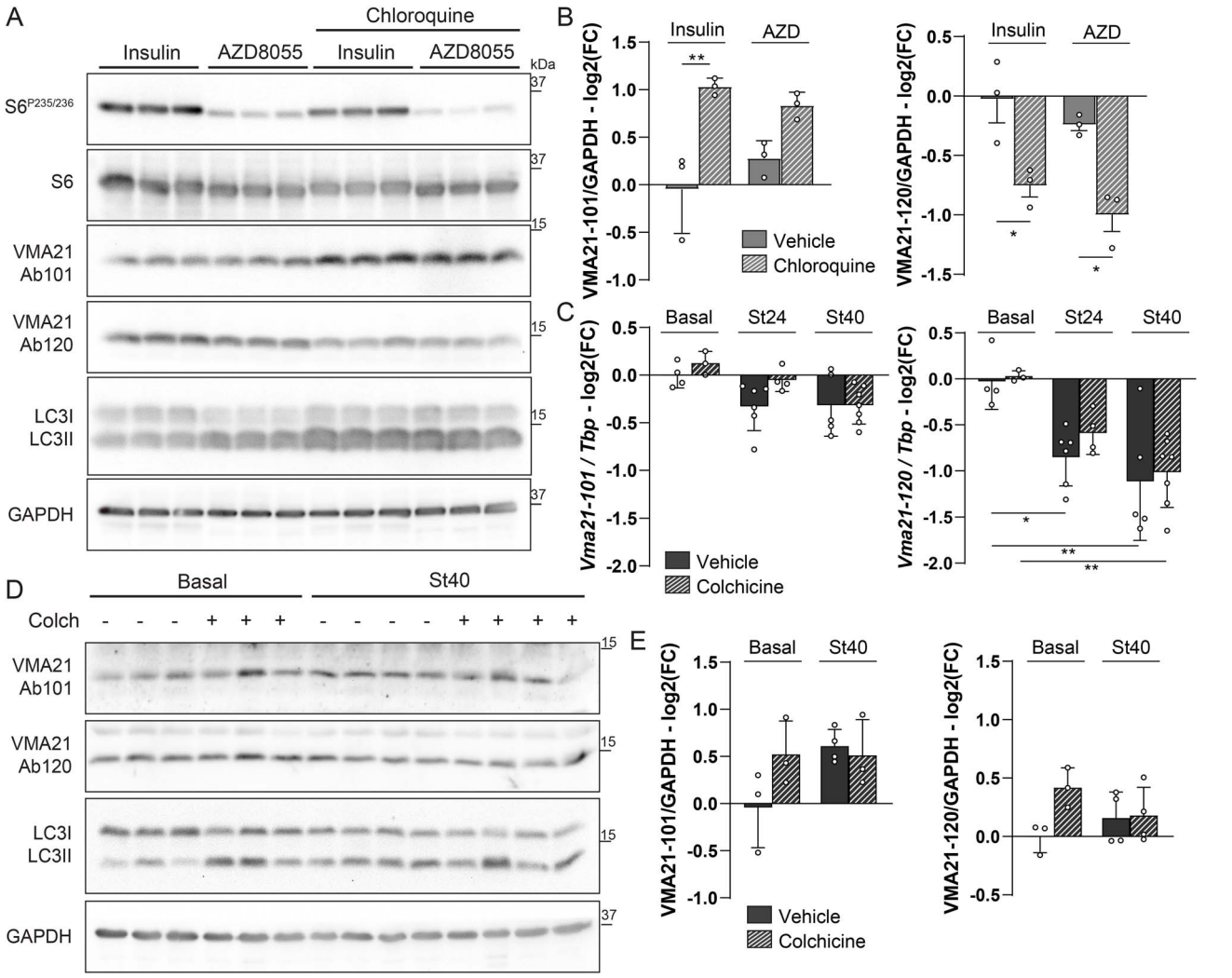

Figure 5. VMA21 expression is not governed by autophagic changes. (A and B) Western blot analysis of VMA21 isoforms in C2C12 myotubes treated with insulin and/or AZD8055. Chloroquine was used to block degradation steps. Protein levels are normalized to GAPDH, and relative to insulin-treated cells. Quantification is given in B. (C) mRNA levels of *Vma21-101* and *Vma21-120* in TA muscle from 3-month-old mice in basal conditions or subjected to 24 h (St24) or 40 h (St40) of starvation. Colchicine was used to block autophagy degradation. Levels are relative to *Tbp* mRNA and to basal conditions. (D and E) Western blot analysis of VMA21 isoforms in TA muscle from 3-month-old mice in basal conditions or subjected to 40 h of starvation (St40). Colchicine (Colch) was used to block autophagy degradation. Protein levels are normalized to GAPDH, and relative to basal conditions. Quantification is given in E. All values are mean ± SD; n = 3 in B; n = 4/3 (basal), 6/4 (St24), 5/7 (St40) in C (−/+ Colch); 3 (basal) and 4 (St40) in E; *p < 0.05, **p < 0.01, two-way ANOVA with Tukey's post-hoc analysis.

VMA21-120 also co-localized with an ERGIC marker in myotubes (Fig. 6B), suggesting that VMA21-120 primarily resides within the ER, COPII vesicles and the ERGIC in muscle cells. Similar to VMA21-101, VMA21-120 did not co-localize with markers for Golgi, COPI, mitochondria or lysosomes (Supplementary Material, Fig. S6C). Interestingly, VMA21-101 displayed a striated staining pattern in mature muscle fibers, comparable to that of the longitudinal SR marker SERCA1, with strong accumulation at I and M bands, corresponding to short and long longitudinal SR, respectively (Fig. 6C). VMA21-120 also co-localized with SERCA1 in short longitudinal SR, but could not be detected at the M band, as observed for KDEL (Fig. 6C and Supplementary Material, Fig. S6D). Using sub-cellular fractionation by ultracentrifugation, we further confirmed that VMA21-101 and -120 are primarily located in the SR/ER within muscle cells (Supplementary Material, Fig. S6E).

Whereas previous reports suggest that VMA21 interacts with the V0c" sub-unit of the v-ATPase [6], recent cryoEM data demonstrated that yeast Vma21p rather interacts with c sub-units of the V0 domain [10]. As VMA21-101 and -120 were both detected in the ER/SR of muscle cells, we tested their capacity to bind V0c/c" sub-units. To this end, we immunoprecipitated VMA21-101 in myoblasts and VMA21-120 in myotubes. The V0c sub-unit co-immunoprecipitated with VMA21-101 in myoblasts (Fig. 6D) and with VMA21-120 in myotubes (Fig. 6E), while V0c" was undetected in IP eluates for both isoforms (Fig. 6D and E). In support of an interaction between VMA21-120 and V0c, overexpressed VMA21-120, but not VMA21-101, co-immunoprecipitated with V0c in C2C12 myoblasts (Fig. 6F). Importantly, VMA21-101 was detected when immunoprecipitating endogenous VMA21-120 from myotubes (Fig. 6E), suggesting that the two isoforms interact, whether directly or indirectly. Hence, by binding the V0 domain of the v-ATPase and/or VMA21-101, VMA21-120 is likely to contribute to the regulation of V0 assembly.

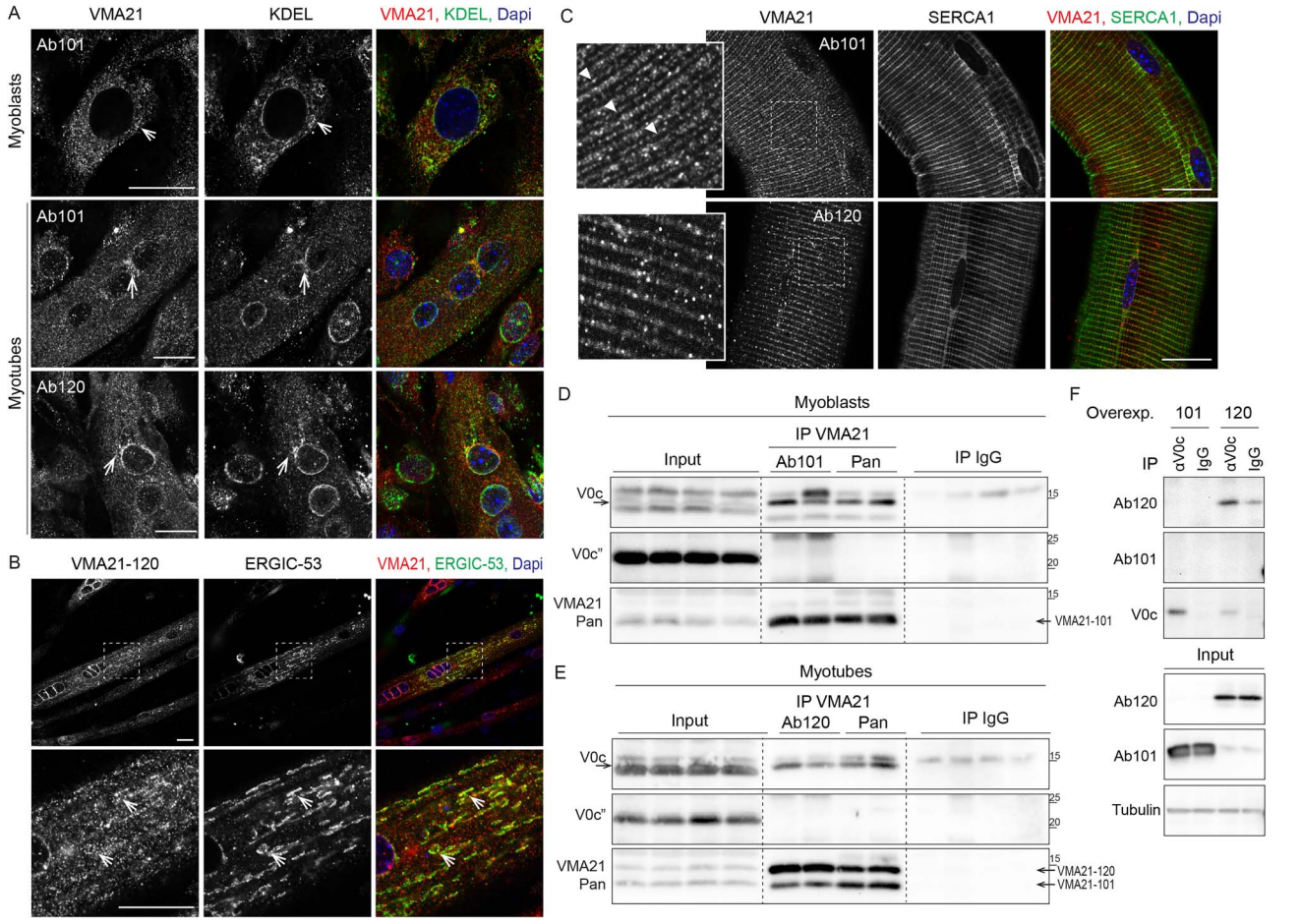

Figure 6. VMA21-101 and VMA21-120 interact with V0c sub-unit in the ER/SR of muscle cells. (A) Immunostaining against VMA21-101 or VMA21-120 shows similar pattern as KDEL marker in C2C12 myoblasts and/or myotubes. Arrows point to perinuclear regions with accumulation of VMA21 and KDEL. Scale bar, 20 μm. (B) VMA21-120 co-localizes with ERGIC-53 overexpressed in C2C12 myotubes. Arrows point to co-localization of VMA21-120 and ERGIC-53. Scale bar, 20 μm. (C) Immunostaining against VMA21-101 or VMA21-120 reveals co-localization with SERCA1 at the I and M (arrowheads) bands of mature muscle fibers. Scale bar, 20 μm. (D and E) V0c sub-unit of the v-ATPase, but not V0c", co-immunoprecipitates (IP) with VMA21-101 and -120 in C2C12 myoblasts (D) and myotubes (E). VMA21-101 co-immunoprecipitates with VMA21-120 in myotubes. (F) VMA21-120, but not VMA21-101, co-immunoprecipitates (IP) with V0c, in C2C12 myoblasts overexpressing VMA21-101 or -120. Levels of tubulin in the input are used as loading control.

VMA21 overexpression does not alter myogenesis or autophagic flux in muscle cells

Previous reports have highlighted the consequences of VMA21 deficiency on autophagy and myogenesis in patient cells [6, 25]. To gain further insight into the roles of each VMA21 isoform, we examined the consequences of their overexpression in muscle cells. Overexpression of VMA21-101 or -120 did not affect C2C12 myoblast proliferation, as measured with EdU pulse and staining (Fig. 7A). Consistently, VMA21-101 transfection did not alter cell growth, monitored with the Incucyte system, compared to GFP-transfected cells (Fig. 7B). More surprisingly, VMA21-120 overexpression increased cell confluency over time (Fig. 7B). As cell proliferation was unchanged, this observation may reflect decreased cell death in VMA21-120-transfected cultures. Transfected myoblasts were then switched to differentiation medium to evaluate the consequences of VMA21 overexpression on their differentiation capacity. Indices of differentiation (i.e. proportion of nuclei in myosin-expressing cells) and fusion (i.e. the proportion of nuclei in cells with more than two nuclei) were unchanged by VMA21-101 overexpression, compared to GFP-overexpressing cells (Fig. 7C and D). VMA21-120 overexpression also did not affect the differentiation and fusion of C2C12 cells, despite the observed temporal regulation of its expression during myogenesis (Fig. 7C and D).

As VMA21 is suggested to regulate autophagy by controlling v-ATPase assembly, we next assessed whether VMA21 overexpression affects autophagic flux. VMA21 isoforms were overexpressed in C2C12 cells, and autophagy was evaluated in transfected myoblasts with or without chloroquine treatment. Compared to GFP-transfected cells, overexpression of VMA21-101/-120 did not change LC3II levels in untreated myoblasts (Fig. 7E and F). However, the fold change in chloroquine-mediated LC3II accumulation was curtailed in VMA21-120-transfected compared to GFP-transfected cells (Fig. 7F). Therefore, high levels of VMA21-120 may limit degradation steps and/or autophagy induction. Consistently, VMA21 deficiency has been shown to indirectly increase autophagy induction, by inhibiting mTORC1 activity [6]. While phosphorylation of the mTORC1 target, S6, tended to increase in VMA21-101-transfected cells, it was unchanged in VMA21-120-transfected cells, compared to GFP-

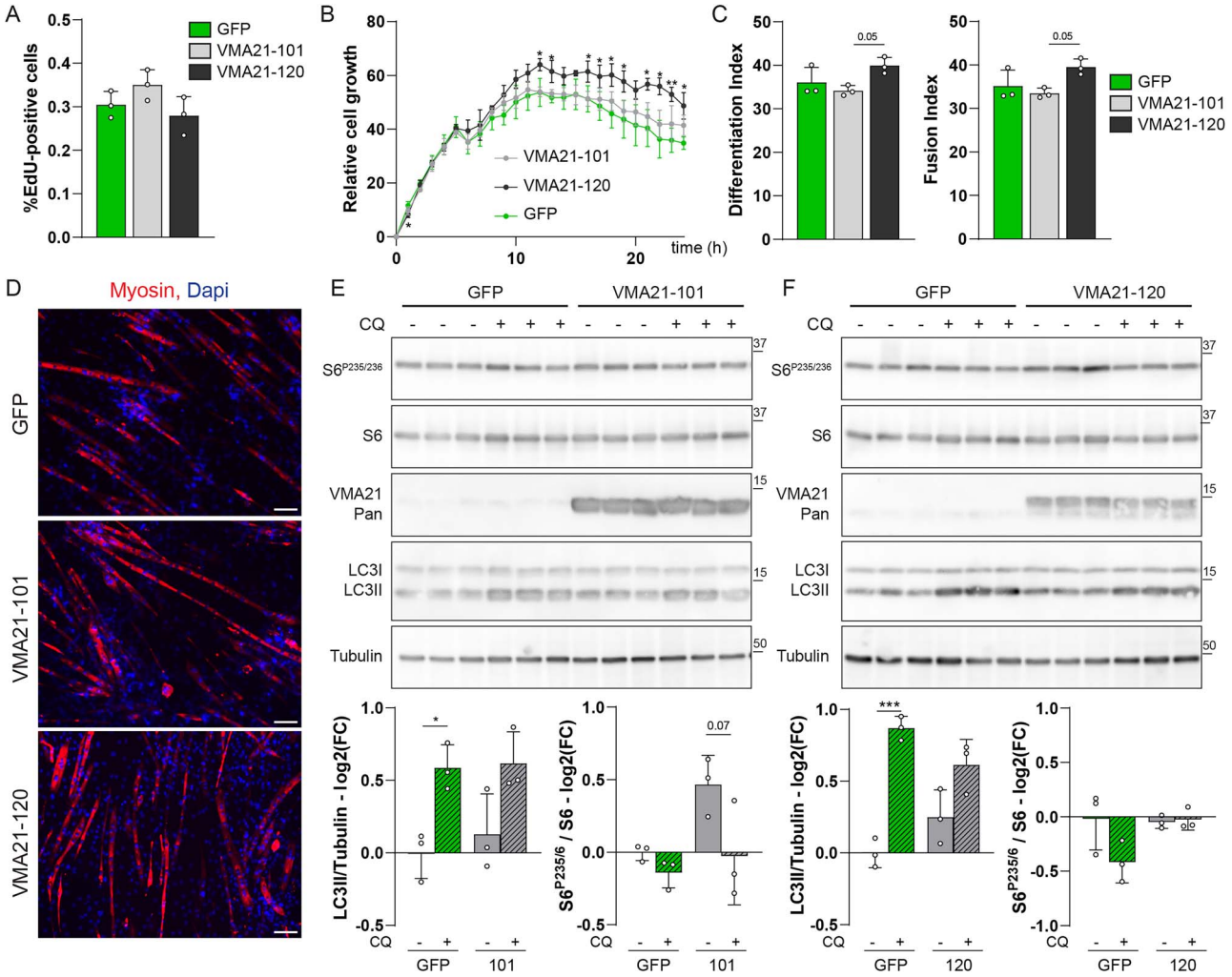

Figure 7. Overexpression of VMA21 has minor effect on muscle cell dynamics and autophagic flux. (A) Overexpression of VMA21-101/-120 in C2C12 myoblasts does not affect the proportion of proliferating cells, identified with EdU staining. (B) Cell growth is increased in VMA21-120-overexpressing cells, as compared to GFP- and VMA21-101-transfected myoblasts. Cell growth was followed over 24 h and evaluated based on cell confluency with Incucyte. (C and D) Overexpression of VMA21-101 or VMA21-120 does not affect the differentiation and fusion capacities of C2C12 cells (C). The indices were calculated based on myosin and Dapi staining (D). Scale bar, 100 μm. (E and F) Western blot analysis of LC3 and S6 levels upon VMA21-101 (E) or VMA21-120 (F) overexpression in C2C12 myoblasts. Chloroquine (CQ) was used to block degradation steps. Levels of LC3II are normalized to tubulin and relative to GFP-transfected untreated cells. Levels of the active phosphorylated form of S6 are normalized to total S6 levels and relative to GFP-transfected untreated cells. All values are mean ± SD; n = 3; *p < 0.05, ***p < 0.001, two-way ANOVA with Tukey's post-hoc analysis.

transfected cells (Fig. 7E). Overall, these results indicate that increasing VMA21 amount has limited effects on cell dynamics or autophagic flux in muscle cells.

Expression of VMA21 isoforms is altered in cells from XMEA patients

To evaluate the pathophysiological relevance of the muscle-specific VMA21 isoform identified in mice, we assessed the expression pattern of VMA21-101 and VMA21-120/156 in human muscle cells. RNAseq data [18, 19] suggest that *VMA21-101* is expressed strongly in all human cells, while *VMA21-120/156* expression is limited to muscle cells, but at lower levels than those observed in mice (Supplementary Material, Fig. S7). We first quantified the expression of *VMA21* transcripts in primary human myoblasts and myotubes after 4 days of differentiation by qPCR (Supplementary Material, Fig. S8A). As observed in mouse cells, total *VMA21* mRNA levels increased upon differentiation (Fig. 8A). Relative to total *VMA21* levels, *VMA21-101* levels remained unchanged (Fig. 8B), while the expression of *VMA21-120/156* increased strongly upon differentiation (Fig. 8C). At the protein level, VMA21-101 expression was comparable between myoblasts and myotubes (Fig. 8D). In contrast, we detected a strong accumulation of VMA21-120 (i.e. around 14 kDa) in human myotubes, while the corresponding band was barely detectable in myoblasts. A weaker band observed below 20 kDa in human myotubes may correspond to VMA21-156 (Fig. 8D). To confirm these results, we conducted immunoprecipitation with the Ab120 antibody on protein lysate from human muscle cells. In these conditions, a band corresponding to VMA21-120, as well as a fainter one corresponding to VMA21-156, were detected in human myotubes, and to a lesser extent in myoblasts (Fig. 8E). This indicates that human muscle cells predominantly express VMA21-120, and at lower levels VMA21-156. VMA21-101 and VMA21-120 proteins were also detected in skeletal muscle tissue from human control individuals (Supplementary Material, Fig. S8B).

Mutations identified in the *VMA21* gene in XMEA and CDG patients lead to reduced *VMA21* gene expression and/or lower VMA21 protein levels [6, 13, 16, 25, 26]. Where specified, the

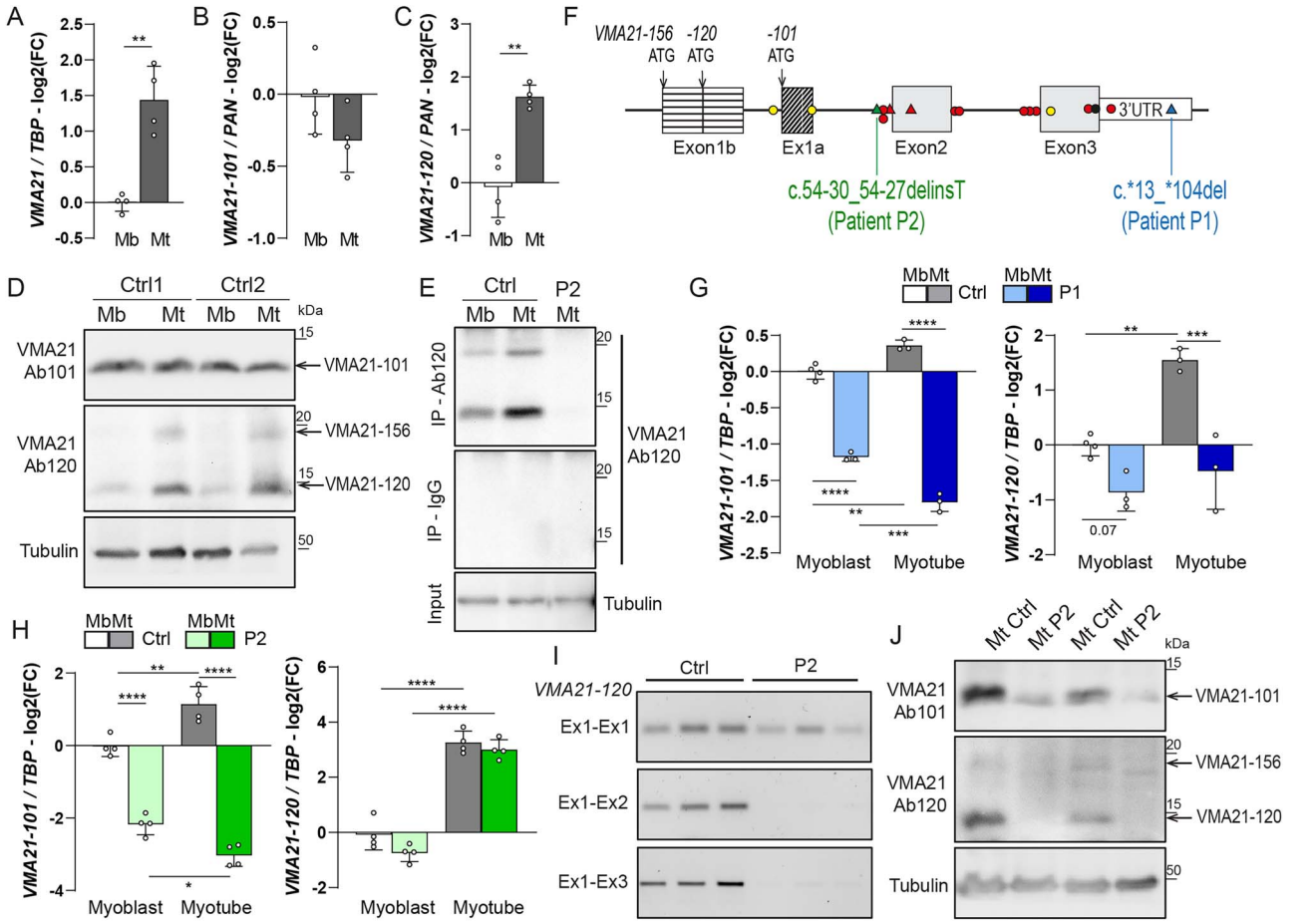

Figure 8. *VMA21* mutations abrogate VMA21-120 expression in muscle cells from XMEA patients. (A-C) Levels of total *VMA21* (A), *VMA21-101* (B) and *VMA21-120/156* (C) transcripts in human primary myoblasts (Mb) and 4-days-differentiated myotubes (Mt). Levels are relative to *TBP* (A) or to total *VMA21* mRNA (B and C), and normalized to myoblasts. Primers used for the qPCR are shown in Supplementary Material, Fig. S8A. (D) Western blot analysis of VMA21 isoforms in human primary myoblasts (Mb) and myotubes (Mt—4 days of differentiation) from two control individuals (Ctrl). (E) Immunoprecipitation (IP) of VMA21-120 with Ab120 in human primary myoblasts (Mb) and myotubes (Mt) from control individual (Ctrl) and XMEA patient (P2). Tubulin is used as a loading control. (F) Scheme showing the localization of *VMA21* mutations identified in XMEA (red), CDG (yellow) and lymphoma (black) patients. Circles and triangles represent nucleotide substitution and deletion, respectively. The mutations corresponding to the two XMEA cell lines used in the study are shown in blue and green. (G and H) Levels of *VMA21-101* and *VMA21-120* transcripts in transduced (G) or primary (H) myoblasts (Mb) and myotubes (Mt) from the XMEA patients P1 (G) and P2 (H). Levels are relative to *TBP* and normalized to control myoblasts. Primers used for the qPCR are shown in Supplementary Material, Fig. S8A. (I) PCR shows amplification of *VMA21-120* exon (Ex) 1, while the amplicons corresponding to exons1-2 or exons1-3 are not detected in myotubes from P2. (J) Western blot analysis of VMA21 isoforms in human primary myotubes (Mt) from control individual (Ctrl) and XMEA patient (P2). Tubulin is used as a loading control. All values are mean ± SD; n = 4 (A–C, H); n = 3 in G (except for Mb Ctrl, n = 4). *p < 0.05, **p < 0.01, ***p < 0.001, ****p < 0.001, Student's t-test (A–C) or two-way ANOVA with Tukey's post-hoc analysis (G and H).

primers and antibodies used in these reports recognized either both isoforms or the VMA21-101 isoform specifically [13, 25]. To evaluate the role of VMA21-120 in XMEA, we examined transcript and protein levels of VMA21 isoforms in cells from two XMEA patients. First, we used fibroblasts and MyoD-transduced myoblasts from an Italian XMEA patient carrying the mutation c.*13_*104del in the 3'UTR region of *VMA21* (P1 patient; Fig. 8F). Second, primary myoblasts were obtained from a Brazilian XMEA patient, carrying the mutation c.54-30_54-27delinsT in intron 1 (P2 patient; Fig. 8F). For both mutations, previous reports suggest reduced VMA21-101 levels [13, 25]. Quantitative RT-PCR using pan primers confirmed reduced total *VMA21* expression in cells from P1 and P2 (Supplementary Material, Fig. S8C–E). Levels of *VMA21-101* were decreased in myoblasts and myotubes from P1 (Fig. 8G) and P2 (Fig. 8H). Interestingly, using specific primers targeting exon 1 of *VMA21-120*, expression was strongly reduced in myotubes from P1 (Fig. 8G), but not in myotubes from P2, compared to control cells (Fig. 8H). Interestingly, after treatment with cycloheximide, a well-known inhibitor of translation used to prevent mRNA decay, both *VMA21-101* and *VMA21-120* transcripts accumulated in P1 myotubes, reaching similar levels as control myotubes (Supplementary Material, Fig. S8F and G). This supported previous reports suggesting that the deletion within the 3'UTR region in P1 reduces *VMA21* transcript stability. To further examine whether *VMA21-120* transcript expression is preserved in myotubes from P2, we assessed its expression by semi-quantitative RT-PCR. Indeed, primers within exon 1 of *VMA21-120* led to similar amplification of the transcript in myotubes from P2 and control cells (Fig. 8I). In contrast, when using primers targeting exon 1—exon 2 or exon 1—exon 3, *VMA21-120* amplification was barely detected in P2 (Fig. 8I). This suggests that the c.54-30_54-27delinsT mutation leads to expression of an alternative *VMA21-120* transcript containing exon 1, but not exons 2 and 3. Using primers specifically targeting the junction between *VMA21-120* exon 1 and the following intron, there was a significant increase in transcript levels in P2 myotubes

compared to controls (Supplementary Material, Fig. S8H). This suggests that the mutation c.54-30_54-27delinsT in intron 1 alters *VMA21-120* expression by impairing transcript splicing and maturation in P2 myotubes. Consistent with the loss of full-length *VMA21-101* and *-120* transcripts, the corresponding proteins were not detected by Western blot in myotubes from P2 (Fig. 8J) or after Ab120 immunoprecipitation (Fig. 8E). Moreover, we did not detect shorter proteins that may arise from translation of *VMA21-120/-156* exon 1 (expected size of 4.2 and 8.3 kDa, respectively; Supplementary Material, Fig. S8I). Hence, VMA21-101 deficiency and VMA21-120 loss may both contribute to muscle pathology in these two XMEA patients.

Discussion

Mutations in the *VMA21* gene cause an autophagic vacuolar myopathy (XMEA) affecting skeletal muscles [7] and a congenital glycosylation disease (CDG) affecting liver [16]. The underlying mechanism dictating tissue specificity in these diseases is unknown. In this study, we show that two isoforms account for the majority of VMA21 expression in humans and mice, with one isoform predominantly expressed in skeletal muscle tissue. Both isoforms were lost in XMEA patients, suggesting that muscle-specific VMA21 isoform deficiency plays a central role in XMEA disease pathogenesis.

VMA21 was first described in yeast as a v-ATPase chaperone [8, 27, 28]. While a single isoform was reported in yeast, we show that two proteins, VMA21-101 and VMA21-120, are expressed in humans and mice. Importantly, we discovered that VMA21-101 is ubiquitously expressed, while VMA21-120 is predominantly expressed in skeletal muscle. The existence of two distinct VMA21 isoforms, with tissue-specific expression patterns, raised the possibility of isoform-specific functions in muscle and non-muscle cells. Previous reports have shown that VMA21 resides within the ER [6, 17], where it chaperones v-ATPase V0 domain assembly. Here, we demonstrate that VMA21-101 and VMA21-120 both reside in the longitudinal SR of mature muscle fibers and interact with the v-ATPase V0c sub-unit. Therefore, VMA21-101 and VMA21-120 may both serve as chaperones for the v-ATPase in muscle cells. The VMA21-101 and VMA21-120 isoforms differ in their N-terminal sequences, which do not contain functionally identified domains. These distinct regions may constitute flexible cytosolic domains that can modulate the binding affinity of VMA21's two transmembrane helices to the different V0 domain sub-units [10]. Of note, concomitant to high VMA21-120 levels, VMA21-101 expression was relatively low in skeletal muscle compared to non-muscle tissues. The balance between the two isoforms, rather than their absolute expression, may be thus functionally important. VMA21-101 and VMA21-120 co-precipitated in myotubes, suggesting a direct or indirect interaction between the two isoforms. One could therefore hypothesize that VMA21-120 either potentiates or impedes the activity of VMA21-101 toward the v-ATPase.

The v-ATPase plays a key role in lysosomal acidification, thereby ensuring autophagic degradation activity [11]. Autophagy induction largely failed to perturb VMA21-101/-120 levels in muscle cells *in vitro* and *in vivo*. On the other hand, autophagy blockade using chloroquine reduced VMA21-120 and increased VMA21-101 levels in muscle cells. Chloroquine blocks autophagy by directly impairing lysosomal function [29, 30], potentially stimulating v-ATPase assembly. Therefore, the observed VMA21-101 predominance under autophagy blockade could indicate that VMA21-101 and VMA21-120 compete for v-ATPase binding and regulation. Genetic deficiencies in v-ATPase sub-units impair lysosomal acidification and autophagy [11]. Similarly, VMA21 deficiency (VMA21-101 and/or VMA21-120) increases lysosomal pH and alters autophagic flux in cells from XMEA and CDG patients [6, 16]. We showed that an excess of either VMA21-101 or VMA21-120 had no major effect on muscle cell dynamics or autophagic flux. Therefore, it is unlikely that VMA21-120 inhibits VMA21-101 chaperone activity, or vice versa, as v-ATPase activity and autophagic flux would have been impaired.

Tightly regulated autophagy is crucial for skeletal muscle homeostasis. Moreover, autophagic flux is relatively strong in skeletal muscle compared to non-muscle tissues [31]. The predominant expression of VMA21-120 in skeletal muscle, with barely detectable protein levels in non-muscle tissues, suggests that it may help to sustain high autophagic demand by directly regulating v-ATPase assembly and/or potentiating VMA21-101 activity. Accordingly, VMA21-120 was strongly expressed in fast-twitch glycolytic skeletal muscles, which are suggested to have higher basal and stress-induced autophagic flux [31, 32]. In comparison, oxidative muscles, such as *soleus*, displayed lower VMA21-120 levels. More importantly, we showed that VMA21-120 expression is dynamically regulated during myogenesis, rapidly and strongly accumulating in muscle precursor cells upon differentiation induction. Consistently, we did not detect VMA21-120 in immortalized C2C12 myoblasts in growth medium, while it was detected in sub-populations of primary muscle cells that are more prone to spontaneously commit and differentiate. Similarly, VMA21-120 accumulated in differentiating muscle precursors and nascent muscle fibers during muscle regeneration. The consensus E-box sites identified upstream of *Vma21-120* TSS are likely key regulatory elements that finely tune *Vma21-120* expression in muscle cells, by allowing the binding of myogenic factors, such as Myogenin. The physiological role of VMA21-120 upon muscle cell differentiation remains to be investigated. Increase in autophagic flux is essential for proper muscle cell differentiation [33, 34]. The v-ATPase was shown to regulate cell fate decision and the balance between proliferation and differentiation in different cell types and organisms [35–39]. Moreover, increased v-ATPase expression is associated with several cancers [40]. VMA21-120 may thus be involved in the tight v-ATPase assembly regulation upon commitment of muscle precursors. Alternatively, VMA21-120 may regulate other targets or processes in differentiating muscle cells, and thereby contribute to myogenesis. VMA21-120 overexpression did not perturb muscle cell differentiation *in vitro*. However, abnormally high cell fusion has been previously reported for the muscle cell line corresponding to XMEA patient P2 [25]. Whether this differentiation defect is caused by VMA21-120 deficiency remains to be determined. Of note, mutations in *VMA21*, leading to mis-localization of VMA21 in lysosomes, are associated with increased cell proliferation in lymphoma cases. VMA21 may hence play a key role in cell fate determination, and the regulation of cell cycle exit toward differentiation.

To examine the contribution of the VMA21-120 isoform to *VMA21*-related diseases, we evaluated the expression of VMA21 isoforms in cells from XMEA patients with two distinct mutations. The mutation c.*13_*104del in the 3′UTR of *VMA21* has been previously shown to abrogate VMA21 expression, likely by destabilizing *VMA21* mRNA [13]. We established that both *VMA21-101* and *VMA21-120* are lost in this XMEA cell line. The deletion in their common 3′UTR region likely confers instability to both transcripts, as *VMA21-101* and *VMA21-120* accumulated upon cycloheximide treatment. Although muscle

cell differentiation was not characterized in this cell line, the mutation was associated with an early disease onset and a relatively high severity [13]. In parallel, the mutation c.54-30_54-27delinsT was associated with a more than 90% decrease in total *VMA21* RNA levels and with an altered autophagic flux in muscle cells [25]. We showed that this mutation reduces transcript and protein levels of VMA21-120 in muscle cells. The deletion includes the -27A nucleotide of intron 1, previously reported as the splicing branch point for exon 2 [6]. As *VMA21-101* and *VMA21-120* share exon 2, it is likely that the mutation affects the expression of both transcripts by similarly impairing exon1-101/exon2 and exon1-120/exon2 splicing. Of note, Pegat *et al.* [41] recently reported a down-regulation of the two predicted *VMA21* transcripts, corresponding to *VMA21-101* and *VMA21-120* characterized in the current study, in fibroblasts from an XMEA patient carrying a mutation in intron 2 [41]. Publicly available RNAseq data suggest *VMA21-120* expression is barely detectable in fibroblasts [18, 19]. Whether this mutation abrogates the up-regulation of VMA21-120 in differentiated muscle cells remains to be investigated. Similarly, expression of VMA21-120 has never been evaluated in cells from CDG patients carrying a mutation in *VMA21*. Two CDG mutations were identified upstream and within exon 1 of *VMA21-101* (see Fig. 8A) [16], which may selectively hinder VMA21-101 expression while preserving VMA21-120 expression. This may explain why skeletal muscle is spared in CDG patients. Notwithstanding, the third mutation identified in CDG [16], as well as the mutation associated with follicular lymphoma [17] are found in *VMA21* exon 3, and should therefore affect both isoforms. Similarly, since XMEA mutations abrogate the expression of both isoforms, it is puzzling that the liver (as well as other non-muscle tissues) is not (or less) affected by the loss of the ubiquitous VMA21-101 isoform in XMEA patients. It is even more intriguing given that mutations in *CCDC115* and *TMEM199*, which encode the human homolog of yeast Vma22p and Vma12p, respectively, also lead to CDG predominantly affecting liver [42, 43]. CryoEM analysis has placed the chaperones CCDC115 and TMEM199 upstream of VMA21 in v-ATPase assembly [10]. Similarly, diseases associated with mutations in *ATP6AP1* and *ATP6AP2*, encoding two central v-ATPase accessory proteins, are characterized by liver dysfunction, with immunodeficiency and cognitive impairment [44, 45]. Hence, further investigations are required to understand the pathomechanisms leading to muscle affliction, while preserving non-muscle tissues in XMEA.

In conclusion, our study demonstrated the expression of a muscle-specific VMA21 isoform, which may be a key player in XMEA pathogenesis. Our data provide essential insights to understand the clinical spectrum associated with *VMA21* mutations, and the pathomechanisms leading to muscle and non-muscle phenotypes.

Materials and methods

Animals

Tissues were harvested from C57Bl6 control mice at different ages. For starvation experiments, mice were euthanized *ad libitum* at 10 a.m. ('basal') or after 24 or 40 h with food deprivation ("starvation") but free access to water. In some experiments, mice were injected with colchicine (Sigma-Aldrich, 0.4 mg/kg) as described previously [46]. To induce complete necrosis of TA muscle, $BaCl_2$ (Sigma-Aldrich, 1.2%) was injected into the hind limb anterior compartment of 3-month-old mice [47]. Mice were euthanized 3, 7, or 15 days following injection.

Cell culture and reagents

C2C12 cells were obtained from the American Type Culture Collection (CRL-1772), maintained in Dulbecco's modified Eagle's medium (DMEM, Sigma) supplemented with 20% fetal bovine serum (FBS, Gibco), 1% penicillin-streptomycin (pen/strep, Gibco), and differentiated in DMEM, 2% horse serum (HS, Gibco), 1% pen/strep. Primary mouse myoblasts were obtained as described previously [48]. They were maintained in DMEM GlutaMAX (Gibco) supplemented with 10% HS, 20% FBS, 1% chicken embryo extract (CEE, MP Biomedicals), 1% pen/strep and 0.5 ng/ml β-fibroblast growth factor (βFGF, Gibco) on Matrigel (Corning) -coated cell culture dishes in 37°C incubator with 5% CO_2. To induce myogenic differentiation, cells were switched to DMEM GlutaMAX with 4% HS, 1% CEE and 1% pen/strep. For proliferation assay, the Click-iT™ Plus EdU Cell Proliferation Kit (ThermoFisher) was used. Differentiation and fusion indices were quantified with Fiji Software using a macro adapted from ViaFuse [49]. For cell growth analysis, cells were seeded in 24-well plate and real-time monitored with the Incucyte®S3 system (Sartorius AG). For autophagic flux studies, C2C12 myoblasts and myotubes were incubated for 1 h with insulin (15 nM; Sigma-Aldrich), 2 h with ADZ8055 (80 nM; Sigma-Aldrich), and/or overnight with chloroquine (60 μM; Sigma-Aldrich), diluted in growth or differentiation medium. Human primary myoblasts were maintained in growth medium (M199:DMEM with 1:4 ratio, 20% FBS, 50 μg/ml gentamicin (Gibco), 25 μg/ml fetuin (Gibco), 0.5 ng/ml βFGF, 5 ng/ml EGF (Gibco), 0.2 μg/ml dexamethasone (Sigma-Aldrich), 5 μg/ml insulin), and differentiated in DMEM, 10 μg/ml insulin, 50 μg/ml gentamicin. Primary fibroblasts from control individual were obtained after enzymatic dissociation of muscle biopsy and FACS sorting [50]. Primary and immortalized transduced fibroblasts were grown in DMEM, 10% FBS, 50 μg/ml gentamicin. To induce myogenic conversion, doxycyclin (2 μg/ml; Sigma-Aldrich) was added in the medium [51]. To inhibit translation and prevent mRNA decay, myotubes were treated with cycloheximide (100 μg/ml; Sigma-Aldrich) for 10 h.

In vitro transfection

Plasmids encoding GFP and VMA21 isoforms were from Nepagene and OriGene, respectively. Plasmids were amplified in competent DH5α *E. coli* strain and extracted with the endotoxin-free NucleoBond® Xtra Maxi kit (Macherey Nagel). Transfection of C2C12 cells was done with C2C12 Cell Avalanche (EZ Biosystems) or JetOptimus (Polyplus-transfection), as previously described [52].

Transcript expression analysis

RNAs were extracted with the RNeasy Fibrous Tissue Mini Kit (QIAGEN). End-point and quantitative PCR were performed on DNase-treated RNA, reverse transcribed with the High-Capacity cDNA Reverse Transcription Kit (Applied Biosystems), and amplified with the GoTaq G2 Hot Start Master Mix (Promega) or the Power Up SYBR Green Master Mix (Applied Biosystems). Quantitative PCR were analyzed using Step One software and normalized to *TBP/Tbp, 18 s* or total *VMA21/Vma21* expression. Primers are listed in Supplementary Material, Table S1.

Western blot analysis

Nitrogen-powdered tissues and cells were lysed in RIPA buffer (50 mM Tris HCl pH 8, 150 mM NaCl, 1% NP-40, 0.5% sodium deoxycholate, 0.1% SDS, 1% Triton-X100, 10% glycerol) with Protease Inhibitor Tablets, EDTA-free (Pierce) and phosphatase inhibitor

tablets (Roche). Lysates were incubated on ice for 2 h, sonicated two times for 10 s and centrifuged at 10 000 g for 20 min at 4°C. Cleared lysates were used to determine total protein amount (BCA Protein Assay, Pierce). Subcellular fractionation of muscle cells was conducted as previously described [53] using Dounce homogenization. For immunoprecipitation, cells and tissues were lysed in 50 mM Tris HCl pH 8, 150 mM NaCl, 0.5 mM EDTA, 0.1% Triton-X100. Total lysates (1 mg of protein) were incubated successively with primary antibodies or control IgG, and with protein A/G magnetic beads (Pierce), before being washed in 50 mM Tris pH 8, 0.05% Tween-20. Proteins were eluted in 50 mM Tris HCl pH 6.8, 2% SDS, 10% glycerol, 0.01% bromophenol blue, 1% 2-mercaptoethanol. Proteins were separated in polyacrylamide SDS gels and transferred to nitrocellulose membrane (Amersham). The loading control was adapted depending on the condition.

Immunostaining

For immunostaining, cells were fixed with prewarmed PBS, 2% PFA, 2% sucrose, washed with PBS, glycine 0.1 M, and blocked in PBS, 3% IgG free bovine serum albumin (BSA, Jackson ImmunoResearch). Muscle sections were blocked in PBS, 3% BSA, without fixation or with prior fixation with 100% cold acetone. For Pax7 and Myogenin, sections were fixed with 4% PFA and 100% methanol, before microwave oven antigen retrieval. Single fibers were isolated from PFA-fixed muscle and permeabilized with PBS, 3% BSA, 0.5% triton, as previously described [46]. Cells, sections and fibers were sequentially incubated with primary and secondary fluorescent antibodies (Jackson ImmunoResearch), and mounted with Vectashield DAPI (Vector Laboratories). Antibodies are listed in Supplementary Material. Images were captured using Zen 2.6 software with Zeiss Axio Imager M2, Zeiss Axio Observer Z1, or Axio Imager Z2 Basis LSM 800 microscopes.

Statistical analyses

Results are expressed as mean ± SD, with n (number of individual experiments) ≥ 3. Statistical comparison was performed using two-tailed Student's t-test or one/two-way ANOVA test dependent on the conditions, with prior log transformation for qPCR data and Western blot quantification. A 0.05 level of confidence was accepted for statistical significance.

Study approval

All animal studies were performed in accordance with the European Union guidelines for animal care and approved by the Veterinary Office of the Canton of Geneva (application number GE15120B/GE220). Fibroblasts and human myoblasts were obtained from the Telethon Network of Genetic Biobanks and the Myoline platform in accordance with European recommendations and Swiss legislation. Human cells were obtained and used in accordance with the guidelines and regulations of the Swiss Regulatory Health Authorities and approved by the Commission Cantonale d'Ethique de la Recherche from the Geneva Cantonal Authorities, Switzerland (protocol no. PB_2016-01793 and 2021-02160).

Acknowledgements

We thank O. Dupont, Prof. M. Vainzof, Dr V. Mouly and the Myoline platform from the Institut de Myologie (Paris, France), as well as the Biobank of Cells, tissues and DNA from patients with neuromuscular diseases, member of the Telethon Network of Genetic Biobanks (Project no. GTB12001), funded by Telethon Italy, and of the EuroBioBank network, for providing human samples. We thank Prof. M. Frieden, Prof. M. Rüegg and Dr Y. Meinard for their comments on the manuscript. We acknowledge B.N. Boersma for his help with the Incucyte S3 analysis, V. Regard for embryo tissues, and Dr A. Carreras Sureda for tissues of aging mice. The antibody for Golgi marker was a gift from Prof. M. Stoeber. The plasmid for ERGIC-53 marker was a gift from Prof. P. Nunes-Hasler. EmbMHC, SERCA1, Desmin, pan MHC and Lamp1 antibodies, developed by H.M. Blau, D.M. Fambrough, D.A. Fischman, and J.T. August, were obtained from the Developmental Studies Hybridoma Bank (University of Iowa, Iowa City, Iowa, USA).

Supplementary data

Supplementary data is available at *HMG Journal* online.

Conflict of interest statement: None declared.

Funding

This work was supported by the Swiss National Science Foundation (PCEFP3_181102).

Data availability

Data generated during the study are freely accessible on the Yareta repository database: https://doi.org/10.26037/yareta:evksg6wmrnbkhcavlhxihjprdu.

References

1. Lu G, Wang Y, Shi Y. *et al.* Autophagy in health and disease: from molecular mechanisms to therapeutic target. *MedComm* 2022;**3**:e150.
2. Mammucari C, Milan G, Romanello V. *et al.* FoxO3 controls autophagy in skeletal muscle in vivo. *Cell Metab* 2007;**6**:458–71.
3. Castets P, Lin S, Rion N. *et al.* Sustained activation of mTORC1 in skeletal muscle inhibits constitutive and starvation-induced autophagy and causes a severe, late-onset myopathy. *Cell Metab* 2013;**17**:731–44.
4. Masiero E, Agatea L, Mammucari C. *et al.* Autophagy is required to maintain muscle mass. *Cell Metab* 2009;**10**:507–15.
5. Castets P, Frank S, Sinnreich M. *et al.* "Get the balance right": pathological significance of autophagy perturbation in neuromuscular disorders. *J Neuromuscul Dis* 2016;**3**:127–55.
6. Ramachandran N, Munteanu I, Wang P. *et al.* VMA21 deficiency prevents vacuolar ATPase assembly and causes autophagic vacuolar myopathy. *Acta Neuropathol* 2013;**125**:439–57.
7. Dowling JJ, Moore SA, Kalimo H. *et al.* X-linked myopathy with excessive autophagy: a failure of self-eating. *Acta Neuropathol* 2015;**129**:383–90.
8. Malkus P, Graham LA, Stevens TH. *et al.* Role of Vma21p in assembly and transport of the yeast vacuolar ATPase. *Mol Biol Cell* 2004;**15**:5075–91.
9. Wang LF, Wu D, Robinson CV. *et al.* Structures of a complete human V-ATPase reveal mechanisms of its assembly. *Mol Cell* 2020;**80**:501–511.e3.
10. Wang H, Bueler SA, Rubinstein JL. Structural basis of V-ATPase V(O) region assembly by Vma12p, 21p, and 22p. *Proc Natl Acad Sci U S A* 2023;**120**:e2217181120.
11. Colacurcio DJ, Nixon RA. Disorders of lysosomal acidification-the emerging role of v-ATPase in aging and neurodegenerative disease. *Ageing Res Rev* 2016;**32**:75–88.

12. Yan C, Tanaka M, Sugie K. *et al.* A new congenital form of X-linked autophagic vacuolar myopathy. *Neurology* 2005;**65**:1132–4.
13. Ruggieri A, Ramachandran N, Wang P. *et al.* Non-coding VMA21 deletions cause X-linked myopathy with excessive autophagy. *Neuromuscul Disord* 2015;**25**:207–11.
14. Blanco-Arias P, Medina Martinez I, Arrabal Fernandez L. *et al.* Severe congenital X-linked myopathy with excessive autophagy secondary to an apparently synonymous but pathogenic novel variant. *Neuromuscul Disord* 2023;**33**:557–61.
15. Munteanu I, Kalimo H, Saraste A. *et al.* Cardiac autophagic vacuolation in severe X-linked myopathy with excessive autophagy. *Neuromuscul Disord* 2017;**27**:185–7.
16. Cannata Serio M, Graham LA, Ashikov A. *et al.* Mutations in the V-ATPase assembly factor VMA21 cause a congenital disorder of glycosylation with autophagic liver disease. *Hepatology* 2020;**72**:1968–86.
17. Wang F, Yang Y, Boudagh G. *et al.* Follicular lymphoma-associated mutations in the V-ATPase chaperone VMA21 activate autophagy creating a targetable dependency. *Autophagy* 2022;**18**:1982–2000.
18. Li D, Hsu S, Purushotham D. *et al.* WashU Epigenome browser update 2019. *Nucleic Acids Res* 2019;**47**:W158–65.
19. Li D, Purushotham D, Harrison JK. *et al.* WashU Epigenome browser update 2022. *Nucleic Acids Res* 2022;**50**:W774–81.
20. Saclier M, Yacoub-Youssef H, Mackey AL. *et al.* Differentially activated macrophages orchestrate myogenic precursor cell fate during human skeletal muscle regeneration. *Stem Cells* 2013;**31**:384–96.
21. Tang H, Macpherson P, Marvin M. *et al.* A histone deacetylase 4/myogenin positive feedback loop coordinates denervation-dependent gene induction and suppression. *Mol Biol Cell* 2009;**20**:1120–31.
22. Cohen TJ, Barrientos T, Hartman ZC. *et al.* The deacetylase HDAC4 controls myocyte enhancing factor-2-dependent structural gene expression in response to neural activity. *FASEB J* 2009;**23**:99–106.
23. Cohen TJ, Waddell DS, Barrientos T. *et al.* The histone deacetylase HDAC4 connects neural activity to muscle transcriptional reprogramming. *J Biol Chem* 2007;**282**:33752–9.
24. Fortini P, Iorio E, Dogliotti E. *et al.* Coordinated metabolic changes and modulation of autophagy during Myogenesis. *Front Physiol* 2016;**7**:237.
25. Fernandes SA, Almeida CF, Souza LS. *et al.* Altered in vitro muscle differentiation in X-linked myopathy with excessive autophagy. *Dis Model Mech* 2020;**13**.
26. Kurashige T, Takahashi T, Yamazaki Y. *et al.* Elevated urinary β2 microglobulin in the first identified Japanese family afflicted by X-linked myopathy with excessive autophagy. *Neuromuscul Disord* 2013;**23**:911–6.
27. Hill KJ, Stevens TH. Vma21p is a yeast membrane protein retained in the endoplasmic reticulum by a di-lysine motif and is required for the assembly of the vacuolar H(+)-ATPase complex. *Mol Biol Cell* 1994;**5**:1039–50.
28. Graham LA, Hill KJ, Stevens TH. Assembly of the yeast vacuolar H+-ATPase occurs in the endoplasmic reticulum and requires a Vma12p/Vma22p assembly complex. *J Cell Biol* 1998;**142**:39–49.
29. Myers BM, Tietz PS, Tarara JE. *et al.* Dynamic measurements of the acute and chronic effects of lysosomotropic agents on hepatocyte lysosomal pH using flow cytometry. *Hepatology* 1995;**22**:1519–26.
30. Mauthe M, Orhon I, Rocchi C. *et al.* Chloroquine inhibits autophagic flux by decreasing autophagosome-lysosome fusion. *Autophagy* 2018;**14**:1435–55.
31. Mizushima N, Yamamoto A, Matsui M. *et al.* In vivo analysis of autophagy in response to nutrient starvation using transgenic mice expressing a fluorescent autophagosome marker. *Mol Biol Cell* 2004;**15**:1101–11.
32. Mofarrahi M, Guo Y, Haspel JA. *et al.* Autophagic flux and oxidative capacity of skeletal muscles during acute starvation. *Autophagy* 2013;**9**:1604–20.
33. McMillan EM, Quadrilatero J. Autophagy is required and protects against apoptosis during myoblast differentiation. *Biochem J* 2014;**462**:267–77.
34. Mizushima N, Levine B. Autophagy in mammalian development and differentiation. *Nat Cell Biol* 2010;**12**:823–30.
35. Tuttle AM, Hoffman TL, Schilling TF. Rabconnectin-3a regulates vesicle endocytosis and canonical Wnt signaling in zebrafish neural crest migration. *PLoS Biol* 2014;**12**:e1001852.
36. Wissel S, Harzer H, Bonnay F. *et al.* Time-resolved transcriptomics in neural stem cells identifies a v-ATPase/Notch regulatory loop. *J Cell Biol* 2018;**217**:3285–300.
37. Pamarthy S, Mao L, Katara GK. *et al.* The V-ATPase a2 isoform controls mammary gland development through Notch and TGF-β signaling. *Cell Death Dis* 2016;**7**:e2443.
38. Lange C, Prenninger S, Knuckles P. *et al.* The H(+) vacuolar ATPase maintains neural stem cells in the developing mouse cortex. *Stem Cells Dev* 2011;**20**:843–50.
39. Ayodele BA, Mirams M, Pagel CN. *et al.* The vacuolar H(+) ATPase V(0) subunit d(2) is associated with chondrocyte hypertrophy and supports chondrocyte differentiation. *Bone Rep* 2017;**7**:98–107.
40. Chen F, Kang R, Liu J. *et al.* The V-ATPases in cancer and cell death. *Cancer Gene Ther* 2022;**29**:1529–41.
41. Pegat A, Streichenberger N, Lacoste N. *et al.* Novel Intronic mutation in VMA21 causing severe phenotype of X-linked myopathy with excessive autophagy-case report. *Genes* 2022;**13**.
42. Jansen JC, Timal S, van Scherpenzeel M. *et al.* TMEM199 deficiency is a disorder of Golgi homeostasis characterized by elevated aminotransferases, alkaline phosphatase, and cholesterol and abnormal glycosylation. *Am J Hum Genet* 2016;**98**:322–30.
43. Jansen JC, Cirak S, van Scherpenzeel M. *et al.* CCDC115 deficiency causes a disorder of Golgi homeostasis with abnormal protein glycosylation. *Am J Hum Genet* 2016;**98**:310–21.
44. Rujano MA, Cannata Serio M, Panasyuk G. *et al.* Mutations in the X-linked ATP6AP2 cause a glycosylation disorder with autophagic defects. *J Exp Med* 2017;**214**:3707–29.
45. Jansen EJ, Timal S, Ryan M. *et al.* ATP6AP1 deficiency causes an immunodeficiency with hepatopathy, cognitive impairment and abnormal protein glycosylation. *Nat Commun* 2016;**7**:11600.
46. Castets P, Rion N, Theodore M. *et al.* mTORC1 and PKB/Akt control the muscle response to denervation by regulating autophagy and HDAC4. *Nat Commun* 2019;**10**:3187.
47. Morton AB, Norton CE, Jacobsen NL. *et al.* Barium chloride injures myofibers through calcium-induced proteolysis with fragmentation of motor nerves and microvessels. *Skelet Muscle* 2019;**9**:27.
48. Castets P, Bertrand AT, Beuvin M. *et al.* Satellite cell loss and impaired muscle regeneration in selenoprotein N deficiency. *Hum Mol Genet* 2011;**20**:694–704.
49. Hinkle ER, Essader TO, Gentile GM. *et al.* ViaFuse: Fiji macros to calculate skeletal muscle cell viability and fusion index. *Skelet Muscle* 2021;**11**:28.
50. Laumonier T, Bermont F, Hoffmeyer P. *et al.* Human myogenic reserve cells are quiescent stem cells that contribute to muscle regeneration after intramuscular transplantation in immunodeficient mice. *Sci Rep* 2017;**7**:3462.

51. Chaouch S, Mouly V, Goyenvalle A. *et al.* Immortalized skin fibroblasts expressing conditional MyoD as a renewable and reliable source of converted human muscle cells to assess therapeutic strategies for muscular dystrophies: validation of an exon-skipping approach to restore dystrophin in Duchenne muscular dystrophy cells. *Hum Gene Ther* 2009;**20**: 784–90.
52. Cocchiararo I, Cornut M, Soldati H. *et al.* Back to basics: optimization of DNA and RNA transfer in muscle cells using recent transfection reagents. *Exp Cell Res* 2022;**421**:113392.
53. Wang WA, Demaurex N. The mammalian trafficking chaperone protein UNC93B1 maintains the ER calcium sensor STIM1 in a dimeric state primed for translocation to the ER cortex. *J Biol Chem* 2022;**298**:101607.